Nucleon Structure Functions, $F_2(x, Q^2)$ and $xF_3(x, Q^2)$, from ν-Fe Scattering at the Fermilab Tevatron

S.R.Mishra

Harvard University, Cambridge, MA, 02138.

Representing the CCFR Collaboration

S.R.Mishra, [1] W.C.Leung, P.Z.Quintas, [2] F.Sciulli,

C.Arroyo, K.T.Bachmann, [3] R.E.Blair, [4] C.Foudas, [5] B.J.King, W.C.Lefmann,

E.Oltman, [6] S.A.Rabinowitz, W.G.Seligman, M.H.Shaevitz

Columbia University, New York, NY 10027

F.S.Merritt, M.J.Oreglia, B.A.Schumm[6]

University of Chicago, Chicago, IL 60637

R.H.Bernstein, F. Borcherding, H.E.Fisk, M.J.Lamm,

W.Marsh, K.W.B.Merritt, H.Schellman, [7] D.D.Yovanovitch

Fermilab, Batavia, IL 60510

A.Bodek, H.S.Budd, P. de Barbaro, W.K.Sakumoto

University of Rochester, Rochester, NY 14627

P.H.Sandler, W.H.Smith

University of Wisconsin, Madison, WI 53706.

---

[1]Present Address: Harvard University, Cambridge, MA 02138.

[2]Address after Jan. 1992: Fermilab, Batavia, IL 60510.

[3]Present address: Widener University, Chester, PA 19013.

[4]Present address: Argonne National Laboratory, Argonne, IL 60439.

[5]Present address: University of Wisconsin, Madison, WI 53706.

[6]Present address: Lawrence Berkeley Laboratory, Berkeley, CA 94720.

[7]Present address: Northwestern University, Evanston, IL 60208.

Abstract: We present precision measurements of nucleon structure functions, $F_2(x, Q^2)$ and $xF_3(x, Q^2)$ from a sample of 1,320,000 ν_μ-Fe and 280,000 $\bar{\nu}_\mu$-Fe high-energy charged current interactions at the Fermilab Tevatron. The CCFR measurements of $xF_3(x, Q^2)$ agree in magnitude but differ in Q^2 dependence, at small x, when compared to the CDHSW data; and show for the first time a Q^2 evolution consistent with PQCD. The xF_3 measurement leads to an accurate determination of the Gross-Llewellyn Smith sum rule: $S_{GLS} = \int_x^1 \frac{xF_3}{x} dx = 2.50 \pm 0.018(\text{ stat.}) \pm 0.078(\text{ syst.})$. Our measurements of $F_2(x, Q^2)$ agree well with those from SLAC (eN) and BCDMS (μN) experiments, and lead to a precise test of the mean-square charge prediction by the Quark Parton Model. These data, however, differ from the CDHSW (νFe) and EMC (μN) data. Measurements of the scaling violation of the CCFR F_2 are also in good agreement with the theory. The preliminary value of $\Lambda_{\overline{MS}}$, from the non-singlet evolution with $Q^2 > 15$ GeV^2, is $213 \pm 29(stat.) \pm 41(syst.)$ MeV.

1: Introduction

High energy neutrino uniquely elucidate hadron structure. The parity-conserving and parity-violating amplitudes of ν-interactions lead to a simultaneous determination of $F_2(x, Q^2)$ and $xF_3(x, Q^2)$. These structure functions, in the standard model, are directly related to the momentum densities of the constituent quarks. The differential cross section for the ν-N charged-current process (CC), $\nu_\mu(\bar{\nu}) + N \rightarrow \mu^-(\mu^+) + X$, in terms of the Lorentz invariant structure functions F_2, $2xF_1$, and xF_3 is:

$$\frac{d\sigma^{\nu(\bar{\nu})}}{dxdy} = \frac{G_F^2 s}{2\pi}\left[\left(1 - y - \frac{Mxy}{2E_\nu}\right) F_2(x, Q^2) + \frac{y^2}{2} 2xF_1(x, Q^2) \pm y(1 - \frac{y}{2})xF_3(x, Q^2)\right], \tag{1}$$

where G_F is the weak Fermi coupling constant, M is the nucleon mass, E_ν is the incident neutrino energy, $s = 2E_\nu M + M^2$ is the ν-N center of mass energy, Q^2 is the square of the four-momentum transfer to the nucleon, the scaling variable $y = \frac{E_{HAD}}{E_\nu}$ is the fractional energy transferred to the hadronic vertex, and $x = \frac{Q^2}{2ME_\nu y}$, the Bjorken scaling variable, is the fractional momentum carried by the struck quark. The structure function $2xF_1$ is expressed in terms of F_2 and $R = \sigma_L/\sigma_T$, the ratio of total absorption cross sections for longitudinal and transverse polarized W bosons by $2xF_1(x, Q^2) = \frac{1+4M^2x^2}{1+R(x,Q^2)} \times F_2(x, Q^2)$. From the sums and differences of the differential cross sections of the ν-N and $\bar{\nu}$-N interactions, the "parity conserving" $F_2(x, Q^2)$ and the "parity violating" $xF_3(x, Q^2)$ structure functions are extracted. In the Quark-Parton Model (QPM), F_2 is the sum of all interacting nucleon constituents; and xF_3 is the difference of quark and anti-quark densities or the valence quark density of the nucleon.

Perturbative QCD predicts the amount of scaling violation (the Q^2 dependence) from the measured x-dependence of structure functions at fixed Q^2, and one additional unknown: the strong coupling parameter, α_s [1]. The magnitude of the measured scaling violations can be directly compared to the predictions, and lead to a precise determination of the QCD mass parameter α_s or $\Lambda_{\overline{MS}}$. One critical prediction is the Q^2-dependence of the non-singlet structure function xF_3, since its evolution is independent of the unknown gluon distribution and, therefore, can be used as an unambiguous test of PQCD. Until now this prediction has not met the test of experimental comparison.[2] Finally, a simultaneous analysis of F_2 and xF_3 permits the delineation of the gluon evolution, and leads to an accurate determination of the gluon structure function.

2: CCFR Detector and ν Beam

Structure functions on an iron target were extracted from data taken by the Columbia-

Chicago-Fermilab-Rochester (CCFR) collaboration during two runs in the Fermilab Tevatron neutrino Quadrupole-Triplet beam (QTB).[3,4,5] The QTB delivered $\overline{\nu}_\mu$ and ν_μ in the ratio of $\approx 1/2$, with energies from 30 to 600 GeV, at the CCFR detector.[6] To ensure hadron shower containment and high track reconstruction efficiency, fiducial cuts were imposed upon the 3.7 million muon triggers: transverse event vertex within a square of 2.54m $\times$ 2.54m, longitudinal event vertex at least 4.4m upstream of the downstream end of the target, and selection on the muon track to assure containment by the toroidal spectrometer. To delineate only regions of high efficiency, two kinematic cuts, $E_\mu > 15$GeV and $\theta_\mu < 0.150$ rad, were also imposed upon the reconstructed muons. After these selections, there remained a CC sample of 1,320,000 ν_μ- and 280,000 $\overline{\nu}_\mu$-induced events — an increase by a factor of 11 (18) in $\nu_\mu(\overline{\nu}_\mu)$ event statistics, and a factor 2.5 increase in mean E_ν, over earlier CCFR Narrow Band Beam (NBB) samples.[7]

Accurate measurements of structure functions in deep inelastic lepton experiments depend critically upon a good understanding of calibrations and energy resolutions. Measurements of the scaling violations are particularly sensitive to miscalibrations of either the hadron or muon energies (E_{had} or E_μ). For example, a 1% miscalibration can cause a 50 MeV mismeasurement of $\Lambda_{\overline{MS}}$, but these errors enter with opposite signs. Thus if both E_{had} and E_μ were in error by the same amount, the error in $\Lambda_{\overline{MS}}$ will be small. Therefore, while it is important that the hadron and muon energy calibrations and resolution functions be well known, it is crucial that the energy scales be cross-calibrated to minimize energy uncertainty as a source of error.

The CCFR detector was calibrated in two detailed test runs, using charged particle beams of well defined momenta.[6] The detector was calibrated using charged particle test beams. A hadron beam, at several different energies, was directed into the target carts at different positions. Each beam particle was momentum analyzed to $\approx 1\%$. These data were used to calibrate the calorimeter to about 1% and to determine the calorimeter resolution function.[6] [In two test runs, separated by three years, the energy calibration constant, normalized to muon response, varied by $\approx 0.3\%$.] Test beam muons were used to calibrate the toroid spectrometer to $\approx (.5\% - .6\%)$, to determine the resolution function for muons, and to keep track of the time-dependent calibration changes of the calorimeter.[6]

The relative calibration of E_{had} to E_μ can be checked from the ν data by plotting $\frac{<E_{vis}>^{DATA}}{<E_{vis}>^{MC}}$ as a function of $y = E_{had}/E_{vis}$. If the hadron and muon energy scales are correct, the ratio will be unity for all y. If not, the two energy scales must be adjusted. To satisfy this constraint, calibration adjustments of $E_\mu \rightarrow E_\mu \times 0.995$ and $E_{had} \rightarrow E_{had} \times 1.016$ were chosen; these adjustments are consistent with the known calibration uncertainty. Figure 1 shows the relative calibration after adjustment by these two parameters. The error on the relative calibration remains ($\approx 0.5\%$) the dominant systematic error in the determination of $\Lambda_{\overline{MS}}$.

3: Absolute and Relative Flux

No direct measurement of the neutrino flux was possible in the QTB. Absolute normalization of the flux, relevant for tests of the QPM sum rule predictions,[2] was chosen so that the neutrino-nucleon total cross-section equaled the world average of the iron target experiments, $\sigma^{\nu N} = (.676 \pm .014) \times 10^{-38}\, cm^2\, E_\nu(GeV)$.[8,9] The relative flux determination, *i.e.*, the ratio of fluxes among energies and between $\overline{\nu}$ and ν_μ, relevant for measurements of scaling violation and tests of Quantum Chromodynamics (QCD) predictions, was determined directly from the neutrino data using two techniques as discussed below.

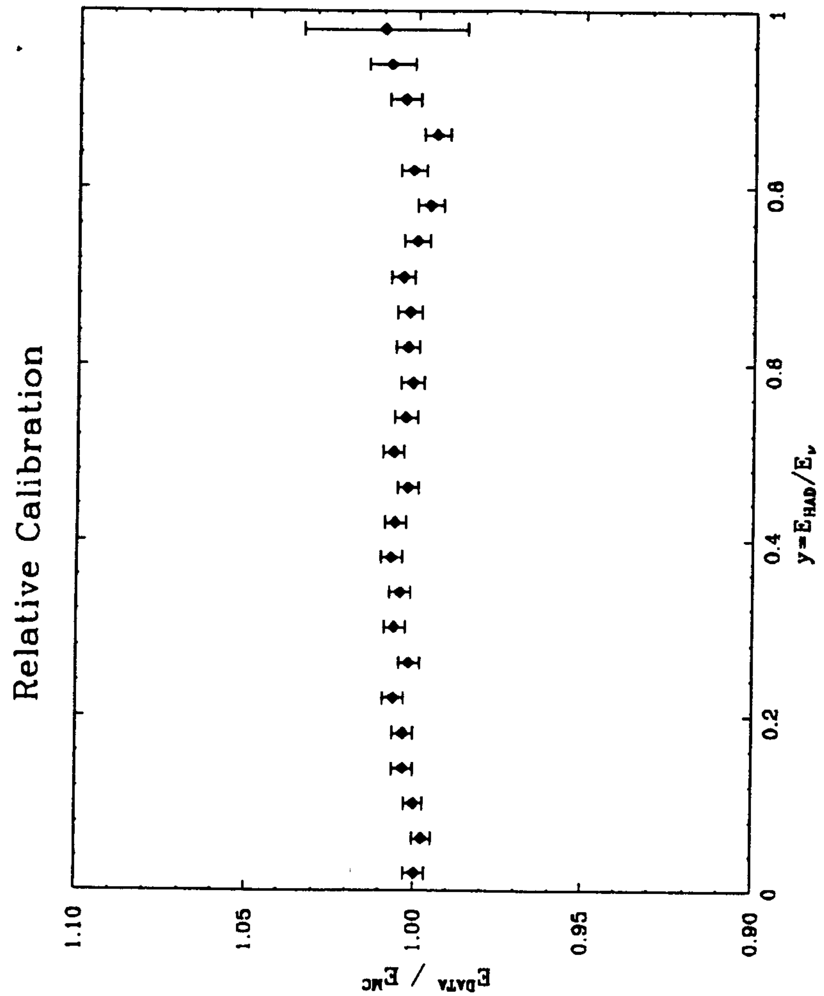

Figure 1: The relative calibration after the adjustment. We plot E_ν^{DATA}/E_ν^{MC} as a function of y. Adjustments of $E_\mu \to E_\mu \times 0.995$ and $E_{had} \to E_{had} \times 1.016$ were made to make the calibration unity for all y.

The two methods used to extract the relative flux $[\Phi(E)]$ were: the fixed ν-cut method and y-intercept method.[10] The two techniques yielded consistent measures of $\Phi(E)$.

The fixed ν-cut method uses the most general form for the differential cross section for the V-A neutrino nucleon interaction which requires that the number of events with $\nu < \nu_0$ in a E_ν bin, $\mathcal{N}(\nu < \nu_0)$, is proportional to the relative flux $\Phi(E_\nu)$ at that bin, up to corrections of order of $\mathcal{O}(\nu_0/E_\nu)$:

$$\mathcal{N}(\nu < \nu_0) = C\Phi(E_\nu)\nu_0\left[\mathcal{A} + (\frac{\nu_0}{E_\nu})\mathcal{B} + (\frac{\nu_0}{E_\nu})^2\mathcal{C} + \mathcal{O}(\frac{\nu_0}{E_\nu})^3\right]. \tag{2}$$

The parameter, ν_0, was chosen to be 20 GeV to simultaneously optimize statistical precision while keeping corrections small. There are 426,000 ν- and 146,000 $\overline{\nu}$-induced events in the fixed ν-cut flux analysis.

The y-intercept method comes from a simple helicity argument: the differential cross sections, $d\sigma/Edy$, for ν- and $\overline{\nu}$-induced events should be equal for forward scattering and independent of energy, *i.e.*, as $y \to 0$.

$$\left[\frac{1}{E}\frac{d\sigma^\nu}{dy}\right]_{y=0} = \left[\frac{1}{E}\frac{d\sigma^{\overline{\nu}}}{dy}\right]_{y=0} = \text{Constant}. \tag{3}$$

Thus, in a plot of number of events versus y, the y-intercept obtained from a fit to the entire y-region is proportional to the relative flux. The fixed ν-cut and y-intercept methods of $\Phi(E)$ determination typically agreed to about 1.5% with no measureable systematic difference. A smoothing procedure was applied to minimize the effects of point-to-point flux variations.[4, 5]

Determination of relative flux permits us to measure the energy dependence of ν_μ- and $\overline{\nu}_\mu$-N total cross sections. (Note that the abosute level of $\sigma(\nu N)$ is assumed from the earlier measurements.) Figure 2a shows the slope of the neutrino cross section, $\sigma^{\nu,\overline{\nu}}/E^{\nu,\overline{\nu}}$ as a function of neutrino energy. Region beyond 220 GeV is new.

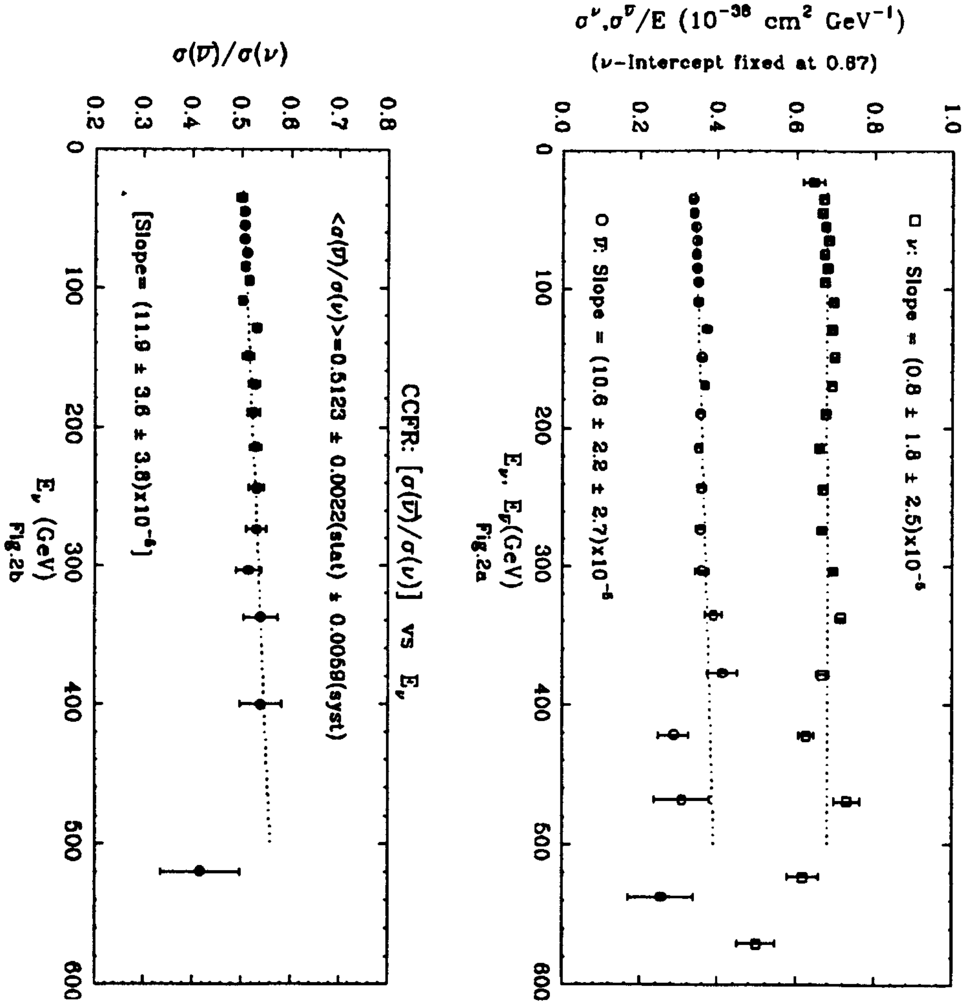

Figure 2a: Energy dependence of ν- and $\bar{\nu}$-N cross sections as a function of E_ν. The rise in $\sigma(\nu - N)/E_\nu$ and $\sigma(\bar{\nu} - N)/E_{\bar{\nu}}$ with energy is consistent with the energy dependent effects. Figure 2b shows the ratio of $\bar{\nu}$-toν cross section as a function of energy.

The observed energy dependence of the cross section slopes are consistent with the known energy dependent effects such as charm theshold, propagator correction, and QCD effects. Figure 2b illustrates the $\sigma(\bar{\nu}N)/\sigma(\nu N)$ as a function of energy. Our measurement leads to a 1% determination of this important ratio.

4: Extraction of Structure Functions

Structure functions were extracted in the kinematic domain $E_{had} > 10$ GeV, $Q^2 > 1$ GeV^2 and $E_\nu > 30$ GeV. In this sample, there were 1,050,000 ν- and 180,000 $\bar{\nu}$-induced events. Accepted events were separated into twelve x bins and sixteen Q^2 bins from 1 to 600 GeV^2. Integrating the ν-N differential cross-section (Eq.1) times the flux over each x and Q^2 bin gives two equations for the number of neutrino and antineutrino events in the bin in terms of the structure functions at the bin centers, x_0 and Q_0^2.

$$\Delta N^{\nu,\bar{\nu}} = (\int a\Phi(E)^{\nu,\bar{\nu}}dE)(\mathrm{F}_2(x_0,Q_0^2)) \pm (\int b\Phi(E)^{\nu,\bar{\nu}}dE)(\mathrm{xF}_3(x_0,Q_0^2)) \qquad (4)$$

where a and b are known functions of x, y, E and $R(x,Q^2)$; and $\Phi(E)$ is the flux. The observed numbers of events, N^ν & $N^{\bar{\nu}}$, were corrected with an iterative Monte Carlo procedure for acceptance and resolution smearing.

To solve these equations for F_2 and xF_3, we assumed a parameterization of $R(x,Q^2)$ determined from the SLAC measurements,[11] and applied corrections for the 6.85% excess of neutrons over protons in iron. We used the magnitude and the x-dependence of the strange sea as determined from our opposite-sign dimuon analysis.[12] The threshold dependence of charm quark production was corrected with the slow rescaling model,[13] where the relevant charm quark mass parameter, $m_c = 1.34 \pm 0.31$GeV, was determined from our data.[12] Radiative corrections followed the calculation by De Rújula *et al.*;[14] and the cross-sections were corrected for the massive W-boson propagator. The charm-threshold, strange sea, and radiative corrections were largely independent of Q^2. For F_2, they ranged from $\pm10\%$ at $x = .015$, to $\pm3\%$ at $x = 0.125$, to $^{+0\%}_{-5\%}$ at $x = 0.65$ over our Q^2 range. For xF_3 they ranged from $^{+4\%}_{-0\%}$ at $x = .015$, to $^{+1.5\%}_{-0\%}$ at $x = 0.125$, to $^{+0\%}_{-6\%}$ at $x = 0.65$. We have excluded the highest x-bin, $0.7 \leq x \leq 1.0$, due to its susceptibility to Fermi motion (which was not included in the smearing correction).

5: $xF_3(x, Q^2)$ Results

5.1: Comparison of the CCFR and the CDHSW Measurements of xF_3

We first present a comparison of our $xF_3(x, Q^2)$ measurements with those reported by the CDHSW collaboration.[15] The magnitudes of the two data agree reasonably well at all x-bins when averaged over Q^2, as shown in Fig.3. The figure presents the ratio of the CDSHW- to the CCFR-xF_3 as a function of x, for $Q^2 > 5$ GeV^2. In each x-bin data were fitted to $A + B \times log(Q^2)$ over an overlapping range of Q^2, and interpolated to the average Q^2 of the CCFR data. The figure illustrates that, within the systematic error of the overall normalization ($\approx 2.5 - 3\%$), the average x-dependence of the two xF_3 measurements are in agreement. There are, however, differences in the Q^2-dependence at fixed x between the two data sets: the logarithmic slopes of xF_3 with respect to Q^2 do not agree well, as illustrated in Fig.4. The xF_3 slope measurements constitute an important test of the QCD prediction. The CDHSW measurement did not agree well with the QCD prediction; it should be noted, however, that the authors stated that the observed discrepancies were within their systematic uncertainties.[15] In contrast, the CCFR measurements of xF_3 clearly corroborate the prediction of QCD as discussed below.

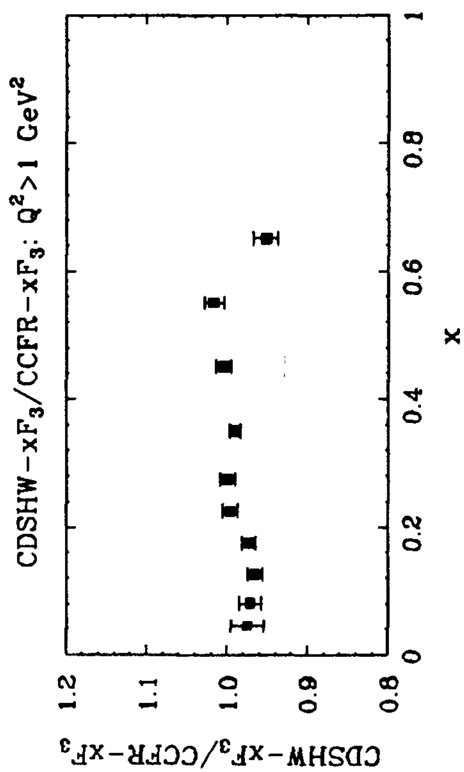

Figure 3: The ratio, CDHSW-xF_3/CCFR-xF_3, with $Q^2 > 1$ GeV^2, as a function of x. Only the statistical errors are shown in Fig.1 through Fig.3.

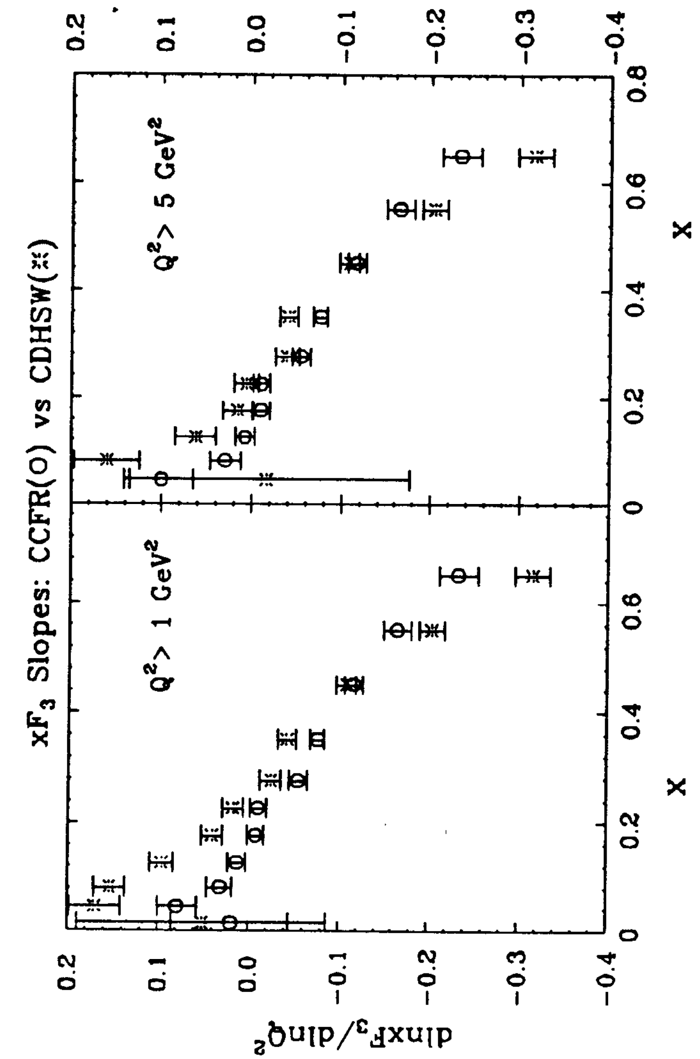

Figure 4: The logarithmic slopes of xF_3 for the CDHSW and CCFR data, with (a) $Q^2 > 1$ GeV^2, and (b) $Q^2 > 5$ GeV^2.

5.2: The Gross-Llewellyn Smith Sum Rule

Measurements of xF_3 lead to a precise test of one of the QPM sum rules, the Gross-Llewellyn Smith (GLS) sum rule. The GLS Sum Rule[16] predicts that the integral of xF_3, weighted by $1/x$, equals the number of valence quarks inside a nucleon — three in the naive quark parton model. With next to leading order QCD corrections, the GLS sum rule can be written as

$$S_{\rm GLS} \equiv \int_0^1 \frac{dx}{x} xF_3(x,Q^2) = 3\left[1 - \frac{12}{(33-2N_f)log(Q^2/\Lambda^2)} + \mathcal{O}(Q^{-2})\right], \quad (5)$$

where N_f is the number of quark flavor (=4) and Λ is the mass parameter of QCD. Higher twist effects, of the order $\mathcal{O}(Q^{-2})$, are expected to be small (< 1% of $S_{\rm GLS}$ at $x \approx 0.01$).[17] Until now, the most precise measurement of the GLS Sum Rule has come from the Narrow Band Beam (NBB) neutrino data of the CCFR collaboration.[7] The factor of 18 increase in the $\overline{\nu}$-induced charged current (CC) sample of the new data, compared to our earlier experiment, provides a much more precise determination of xF_3, and an improved measurement of $S_{\rm GLS}$.

Due to the $1/x$ weighting in Eq.5, the small x region ($x < 0.1$) is particularly important. It follows that the most important issues to assure small systematic errors are (a) accurate determination of the muon angle (θ_μ);[18] and (b) accurate determination of the relative $\overline{\nu}/\nu$ flux. Since xF_3 is obtained from the difference of ν and $\overline{\nu}$ cross-sections, small relative normalization errors can become magnified by the weighting in the integral. The absolute normalization uses an average of ν-N cross-section measurements (see above).

To measure $S_{\rm GLS}$, the values of xF_3 were interpolated or extrapolated to $Q_0^2 = 3$ GeV^2, which is approximately the mean Q^2 of the data in the x-bin which contributes most heavily to the integral. Figure 5 shows the data and the Q^2-dependent fits used to extract $xF_3(x, Q^2 = 3)$ in three x-bins. The resulting xF_3 is then fit to a function

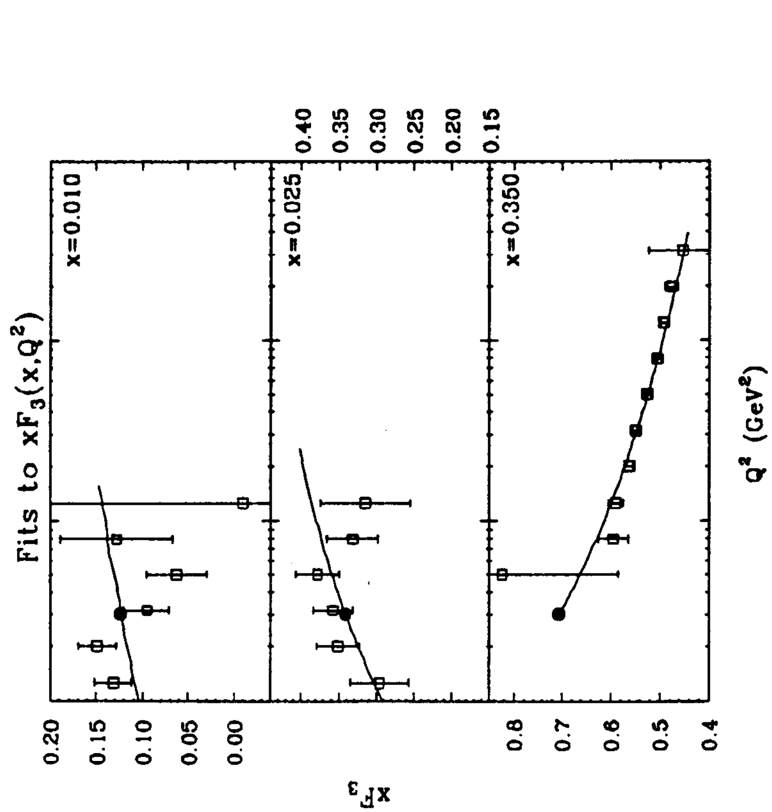

Figure 5: Fits to Q^2-dependence of xF_3 in 3 x-bins (the 2 lowest x-bins and a middle x-bin). xF_3 at $Q_0^2 = 3$ GeV^2 (squares) is obtained by interpolation, as in the 2 lowest x-bin and shown by a dark symbol, or by extrapolation as in the middle x-bin (dark symbol).

of the form: $f(x) = Ax^b(1-x)^c$ $(b > 0)$. The best fit values are $A = 5.976 \pm 0.148$, $b = 0.766 \pm 0.010$, and $c = 3.101 \pm 0.036$. The integral of the fit weighted by $1/x$ gives the $S_{\rm GLS}$. Figure 6 shows the measured $xF_3(x)$ at $Q^2 = 3$ GeV^2, as a function of x, the fits and their integrals. The measurement of the sum rule yields:[19] $S_{\rm GLS} = \int_x^1 \frac{xF_3}{x} dx = 2.50 \pm 0.018(\text{stat.})$.

Fitting different functional forms to our data,[4] gives an answer within $\pm 1\%$ – 1.5% of the above. We estimate ± 0.040 to be the systematic error on $S_{\rm GLS}$ due to fitting. The dominant systematic error of the measurement comes from the uncertainty in determining the absolute level of the flux, which is 2.2%. The other two systematic errors are 1.5% from uncertainties in relative $\bar{\nu}$ to ν flux measurement and 1% from uncertainties in E_μ calibration.[4] The systematic errors are detailed in Table 1. Our value for $S_{\rm GLS}$ is:

$$S_{\rm GLS} = \int_x^1 \frac{xF_3}{x} dx = 2.50 \pm 0.018(\text{ stat.}) \pm 0.078(\text{ syst.}) \, . \tag{6}$$

The theoretical prediction of $S_{\rm GLS}$, for the measured $\Lambda = 213 \pm 50$ MeV from the evolution of the non-singlet structure function,[5] is 2.66 ± 0.04 (Eq.5). The prediction, assuming negligible contributions from higher twist effects, target mass corrections,[20] and higher order QCD corrections, is within 1.8 standard deviation of our measurement. The world status of $S_{\rm GLS}$ measurements is shown in Fig.7.

5.3: The Q^2-Evolution of the Non-Singlet Structure Function

Structure functions evolve in PQCD according to the equations [1]

$$\frac{dF^{NS}(x,Q^2)}{d\ln Q^2} = \frac{\alpha_S(Q^2)}{\pi} \int_x^1 P_{qq}(z,\alpha_s) F^{NS}\left(\frac{x}{z}, Q^2\right) dz \tag{7}$$

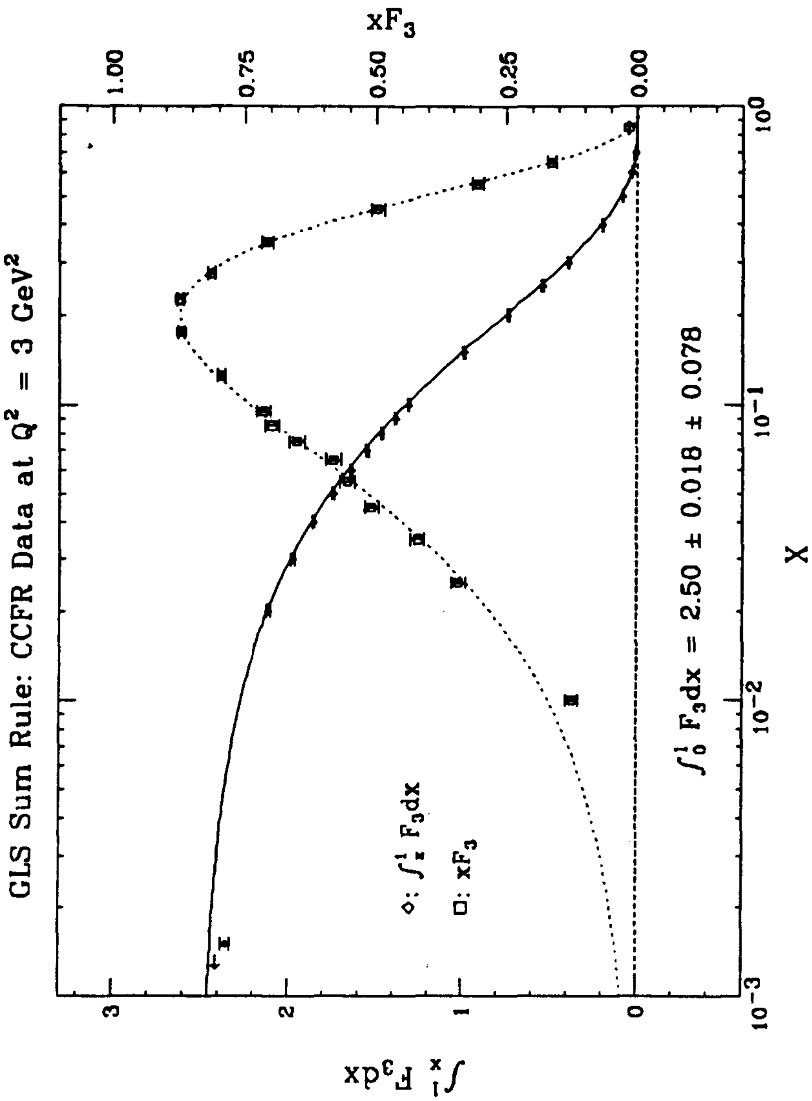

Figure 6: The GLS sum rule: The squares are $xF_3(x,Q^2=3)$ and the dashed line is the fit to $xF_3(x,Q^2=3)$ by $Ax^b(1-x)^c$. The solid line is the integral of the fit, $\int_x^1 \frac{dx}{x} xF_3$. The diamonds are an approximation to the integral computed by a weighted sum $[S(x_i)]$ of $xF_3^j = xF_3(x_j,Q^2=3)$, i.e., $S(x_i) = \sum_j^n \Delta x_j xF_3^j$.

Table 1: **Error on the Gross-Llewellyn Smith sum rule:** The statistical and systematic errors on $S_{\rm GLS}$ are presented.

Error	Variation	ΔS_{GLS}
Statistical		± .018
Systematic		
Fit	different fits	± .040
$\sigma^{\nu N}$ Level	±2.1%	∓ .056
$\frac{\sigma^{\bar{\nu}N}}{\sigma^{\nu N}}$ Level	±1.0%	∓ .034
Energy Scale	±1.0%	± .001
Rel. Calibr.	±0.6%	∓ .010
Flux Shape	smoothing on/off	± .006
Total		± .078

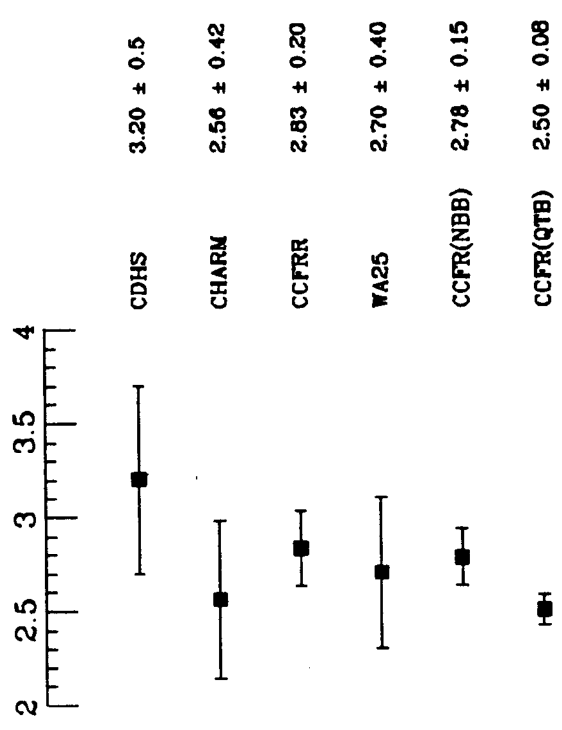

Figure 7: GLS sum rule as measured by previous experiments and these data. The references for other measurements are: CDHS[21a], CHARM[21b], CCFRR[21c], WA25[21d], and CCFR-NBB[3].

$$\frac{dF^S(x,Q^2)}{d\ln Q^2} = \frac{\alpha_S(Q^2)}{\pi}\int_x^1 \left[P_{qq}(z,\alpha_s)F^S(\frac{x}{z},Q^2) + P_{qG}(z,\alpha_s)G(\frac{x}{z},Q^2)\right] dz \quad (8)$$

where the P_{IJ} are the predicted "splitting functions". The non-singlet evolution depends only on the measured structure functions, the known splitting function, and α_s. The singlet equation is more complicated: its evolution is coupled with that of the gluons. Only the non-singlet evolution can be computed without resorting to assumptions about the dependence of the gluons on x and Q^2. Because $P_{qq}(z)$ passes through zero, the left-hand side of Eq.7 is predicted to pass through zero at about $x = 0.11$, independent of α_s. This statement is valid in leading order; in next-to-leading order, all curves parametrized by differing $\Lambda_{\overline{MS}}$ pass through a common point near zero at $x = 0.11$. A comparison of this prediction with experiment is a fundamental test of PQCD which has not yet been demonstrated. The high statistics CDHSW data[15] do not agree well with the predicted dependence of the scaling violations on x, although the authors state that the discrepancies are within their systematic errors. Previous CCFR data lacked the statistical power to offer a conclusive test.[7] The new CCFR data, on the other hand, show an evolution very consistent with PQCD.

We used a modified version of the Duke and Owens program to do a next-to-leading order QCD analysis with target mass correction.[22] Applying cuts on Q^2 to eliminate the non-perturbative region and $x < .7$ to remove the highest x bin (where resolution corrections are sensitive to Fermi motion), best QCD fits to the data were obtained as illustrated in Fig.8 (for $Q^2 > 5$ GeV^2) and discussed below.

Figure 8 shows our new data along with the curve through the points predicted by the theory. A good visual representation of structure function evolution compares the magnitude of the Q^2-dependence of the data in each x-bin with the dependence predicted by the fit. This is shown by plotting the "slopes" ($= \frac{d\ln xF_3}{d\ln Q^2}$) as a function

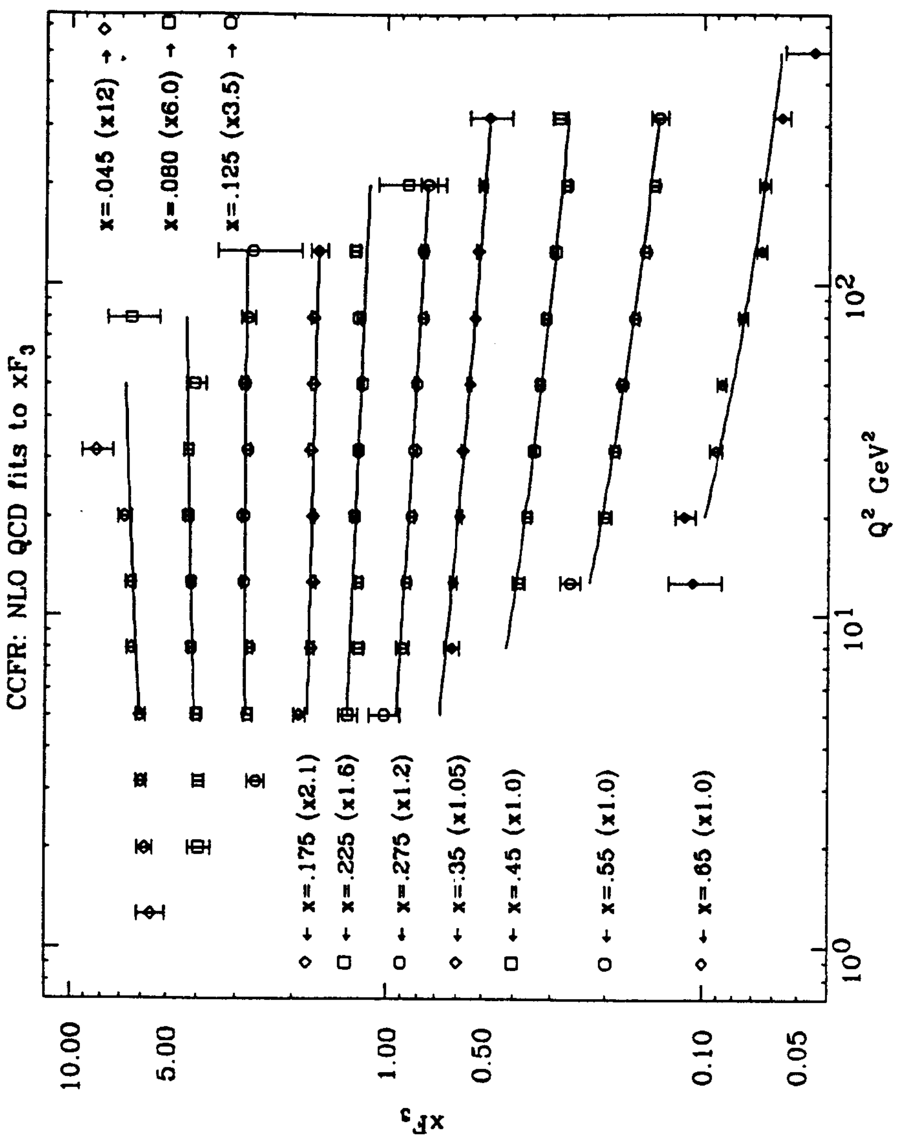

Figure 8: The xF_3 data and the best QCD fit. Cuts of $Q^2 > 5$ GeV^2 and $x < 0.7$ were applied for a next-to-leading order fit including target mass corrections.

of x (Fig.9). More specifically the values shown in Fig.9 result from power law fits to both data and theory over the Q^2 range of the data. The logarithmic slopes of the data agree well with the QCD prediction throughout the entire x-range. This observation is independent of the calibration adjustments. At low-x values the data agree reasonably well with predictions, independent of the value of $\Lambda_{\overline{MS}}$. This is the first confirmation of the QCD prediction for scaling violations in xF_3 which is independent of assumptions about the gluon distributions and is valid over the entire x range.

The value of $\Lambda_{\overline{MS}}$ resulting from the fit was 179±36 MeV, with a χ^2 of 53.5 for 53 degrees of freedom (χ^2=53.5/53). Varying the Q^2 cuts does not significantly change $\Lambda_{\overline{MS}}$; for $Q^2 > 10$ GeV^2, the best fit gives $\Lambda_{\overline{MS}} = 171 \pm 32$ MeV (χ^2=66.4/63); and for $Q^2 > 5$ GeV^2, $\Lambda_{\overline{MS}} = 170 \pm 31$ MeV (χ^2=83.8/80).

A more precise determination of $\Lambda_{\overline{MS}}$ from the non-singlet evolution is obtained by substituting F_2 for xF_3 at large values of x. The evolution of F_2 should conform to that of a non-singlet structure function in a region, $x > x_{cut}$, so long as x_{cut} is large enough that the effects of antiquarks, gluons, and the longitudinal structure function are negligible on its Q^2 evolution. A conservative choice for x_{cut} is one beyond which the antiquarks are consistent with zero. Table 2 shows the antiquark content of the nucleon in our highest x-bins. The table also shows the values of $\Lambda_{\overline{MS}}$ from fits where F_2 was substituted for xF_3 in those bins. (We normalized $F_2(x) = xF_3(x)$ for $x > x_{cut}$; an adjustment of < 3%.) For our best value of $\Lambda_{\overline{MS}}$ from non-singlet evolution we choose to substitute F_2 for xF_3 for $x > 0.5$. (The slopes for F_2 in this region are also shown in Figure 9.) This non-singlet fit yields our best value:

$$\Lambda_{\overline{MS}} = 213 \pm 29 \text{ MeV for } Q^2 > 15 \text{ GeV}^2. \quad (9)$$

The χ^2 for the above fit is 55.3 for 53 degrees of freedom. Varying the x_{cut} from 0.5 to

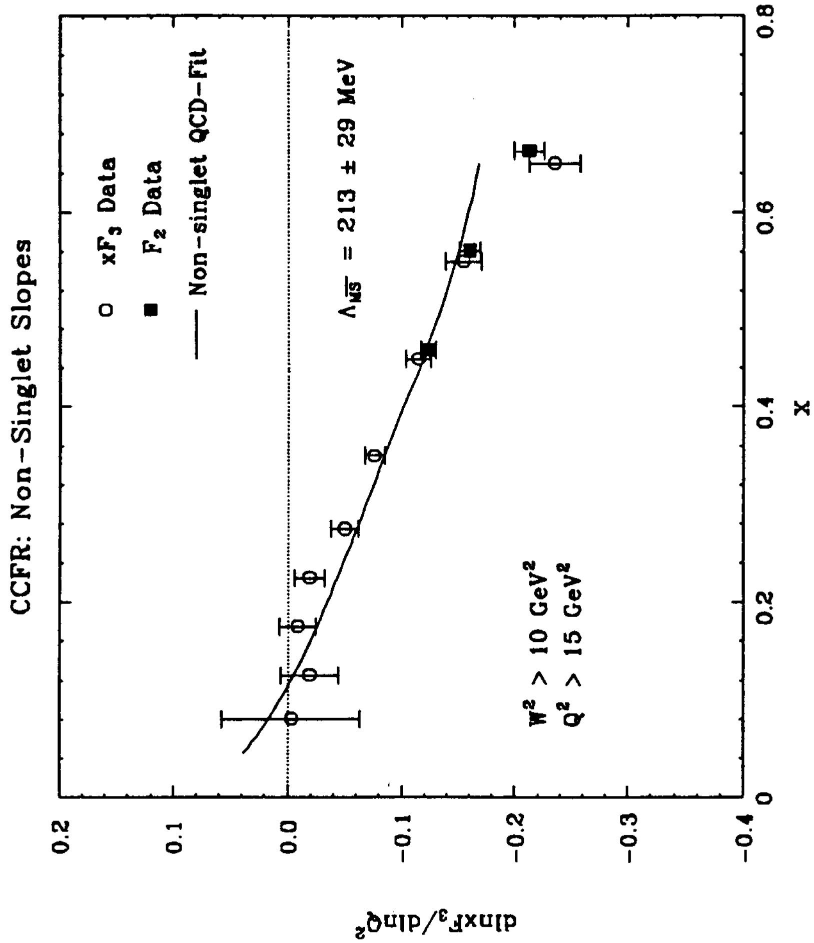

Figure 9: The slopes of xF_3 ($= \frac{d\ln xF_3}{d\ln Q^2}$) for the CCFR data are shown in circles. The curve is a prediction from perturbative QCD with target mass correction. The slopes for F_2 (squares) in the region $x > 0.4$ are also shown (with x values shifted by +2% for clarity).

Table 2: **Antiquarks and Substitution Fits:** Fits are with $Q^2 > 15$ GeV^2, and values of $\Lambda_{\overline{MS}}$ are in MeV. The χ^2/Deg. of freedom (χ^2/dof) is close to unity in all four cases.

x-BIN	$x\bar{q}(x)/xF_3(x)$	$\Lambda_{\overline{MS}}$	χ^2/dof
no substitution		179 ± 36	53.5/53
0.65	−0.3 ± 0.7%	220 ± 34	55.3/53
0.55	1.2 ± 1.0%	213 ± 29	55.3/53
0.45	3.0 ± 0.7%	215 ± 25	50.9/53

0.4 does not significantly change $\Lambda_{\overline{MS}}$; the above substitution yields, $\Lambda_{\overline{MS}} = 215\pm25$ MeV (χ^2=50.9/53). Using $2xF_1$ instead of F_2 in this fit changes $\Lambda_{\overline{MS}}$ by +1 MeV.

The systematic errors on $\Lambda_{\overline{MS}}$ are shown in Table 3. The energy scale error comes from changing both the hadron and muon energies by 1% *in the same direction*. As explained above, the errors from a correlated energy change tend to cancel, resulting in an error of $\approx$ 10 MeV. The largest error comes from a possible miscalibration of E_{had} with respect to E_μ. The statistics of the relative calibration data allow a 0.6% variation of the two energy scales from the ideal which results in a 48 MeV systematic error (36 MeV for the fit with F_2). The last two errors come from varying the two assumptions of the absolute normalization. The fit with xF_3 alone shows a greater dependence on these assumptions because it is formed from differences of neutrino and antineutrino event sums, while F_2 is derived from the sum of the two.

6: $F_2(x,Q^2)$ Results

6.1: The Mean-Square Charge Test

The QPM relates the measurement of F_2 in ν-N scattering to those determined from the charged lepton, e-N or μ-N, scattering. The ratio of the two is a measure of the mean-square quark charge (in units of the square of the electron charge).[2]

$$\frac{F_2^{lN}(x)}{F_2^{\nu N}(x)} = \frac{5}{18}\left(1 - \frac{3}{5}\frac{s+\bar{s}}{q+\bar{q}}\right). \tag{10}$$

Here the small x-dependent correction in parenthesis is due to the asymmetry of the strange and charm sea of the nucleon. The F_2^{lN} data were multiplied by (18/5) times the strange sea correction, and plotted in Fig.10. The comparison of the CCFR-Fe data (solid circle) to those of SLAC-'D' (diamond),[23] BCDMS-'D' (square),[24]

Table 3: Systematic Errors in $\Lambda_{\overline{MS}}$: Values are in MeV. The F_2 data are substituted for xF_3 for $x \geq 0.5$.

ERROR	xF_3 only	$xF_3 + F_2$
Energy Scale	±9	±19
Rel. Calibr.	±48	±36
$\Delta\sigma^{\nu N}$	±11	±6
$\Delta\sigma^{\bar{\nu}N}/\sigma^{\nu N}$	±20	±2
TOTAL SYSTEM	±54	±41

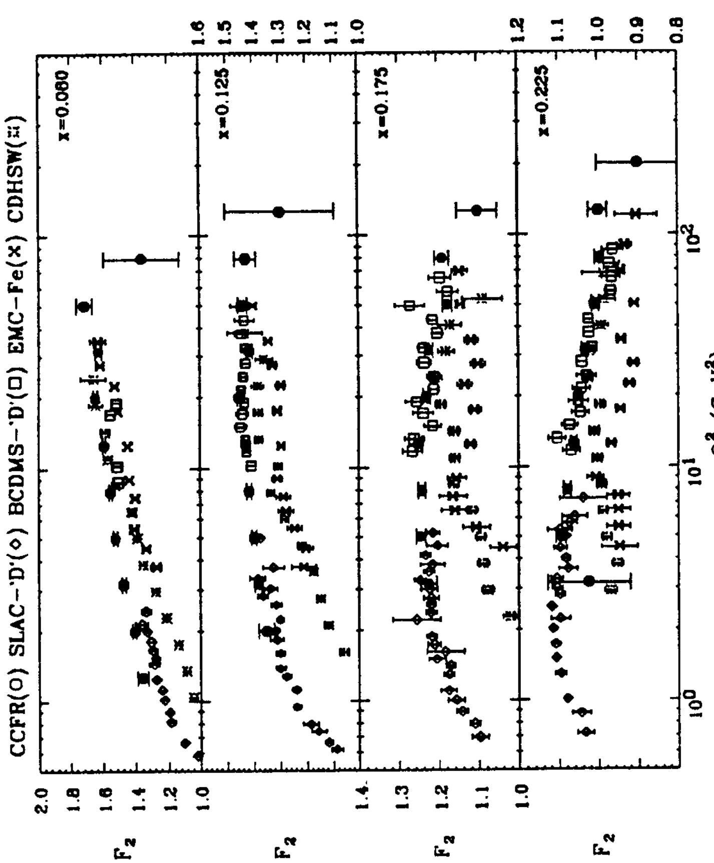

Figure 10: A comparison of $F_2(x, Q^2)$ as a function of Q^2, as measured by the CCFR, SLAC-'D', BCDMS-'D', EMC-Fe, and CDHSW-Fe in a few illustrative x-bins. The deuterium data have been corrected for the EMC-effect using the Fe/D measurement of SLAC. No arbitrary normalization factor is used.

EMC-Fe (cross),[25] and CDHSW-Fe (fuzzy cross)[15] is shown (Fig.10) in a few illustrative x-bins as a function of Q^2. For this comparison, the deuterium data were further corrected for the difference between the light and heavy nuclei using the measured ratio $F_2(Fe)/F_2(D)$ as a function of x.[23] This correction spanned a range from +4% at $x = 0.12$, to -4% at $x = 0.4$, to -12% at $x = 0.6$.

Figure 10 shows good agreement between the SLAC and the CCFR measurements of F_2. These are the first measurements showing substantial overlap with the precise low-Q^2 SLAC data. At higher Q^2, the CCFR data are in good agreement with those of BCDMS-'D', and BCDMS-C data;[24] the latter, however, exist only in the limited range $0.25 \leq x \leq 0.80$, and for clarity are not shown in Fig.10. The EMC-Fe data tend to be systematically lower in magnitude by about 7%; and a display steeper dependence on Q^2 at low x than those of CCFR.

The CDHSW data in the range $0.1 \leq x \leq 0.275$, tend to lie lower than those from this experiment — the disagreement being primarily in the low-Q^2 range of the x-bins. Although the extracted $F_2(x, Q^2)$ depend upon model dependent corrections which are not precisely the same in the two experiments, it should be noted that the corrections in the discrepant x-bins in Fig.10 are no larger than ±2-4%. The origin of this x- and Q^2 dependent disagreement is not understood. The two data sets, however, show better agreement for $x \leq 0.1$ and $x \geq 0.35$.

The mean-square charge test, or the comparison of the CCFR F_2 with those of the muon scattering experiments, is summarized in Fig.11. Data from each μ experiment are corrected using Eq.10, and the muon-to-neutrino F_2 ratio is formed in each x-bin averaged over the overlapping Q^2 range with $Q^2 > 5$ GeV^2. The resulting ratios are plotted as a function of x in Fig.11. It should be noted that the CCFR data span a larger range of than any of the experiments shown in the

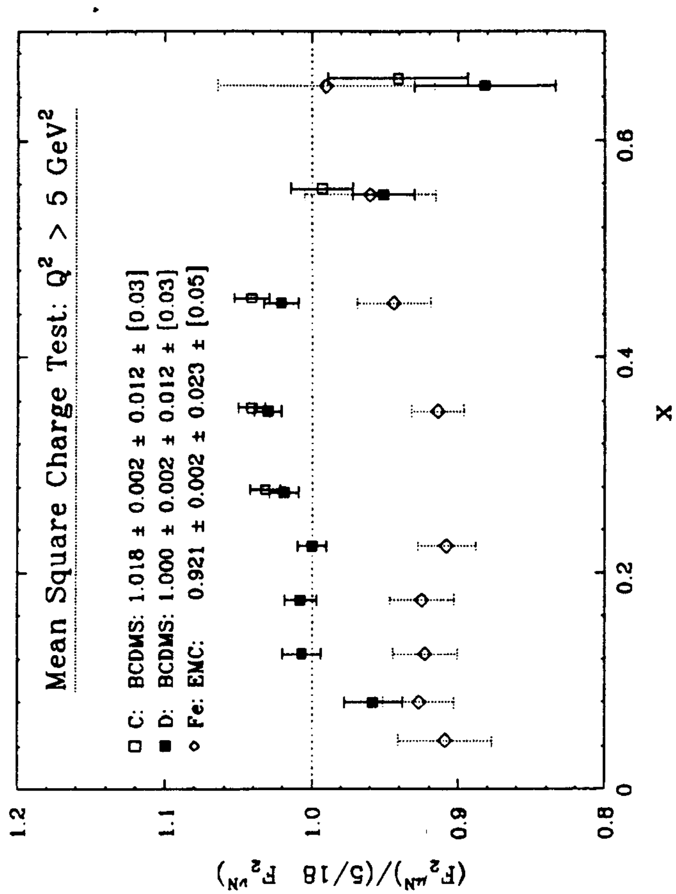

Figure 11: The mean-square charge test with $Q^2 > 5$ GeV^2: The ratio in Eq.10 is shown as a function of x. Systematic errors due to miscalibration and relative normalization of the various experiments dominate the test. The x-independent absolute normalization error is not shown, but is enumerated in Table 1. The BCDMS-C data are shown with x-bins shifted by +1% for clarity.

figure. Systematic errors due to calibration and relative normalization are shown in the figure; absolute normalization errors are not shown. The BCDMS/CCFR ratios are in good agreement with the expected mean square charge. The EMC-Fe/CCFR ratios are systematically lower by about 7% than the prediction, and show reasonable agreement as a function of x; although, due to the averaging over the Q^2 range, the slope discrepancy tends to be obscured. The EMC-'D'/CCFR ratios show similar characteristics and are not shown for clarity in Fig.11. The results of the mean-square charge test are contained in Table 4. The conclusions of this test do not change for a relaxed (> 1 GeV^2), or a more stringent (> 20 GeV^2) Q^2-cut.

6.2: The Q^2-Evolution of the Singlet Structure Function

We have also done preliminary QCD fits evolving F_2, and (F_2 & xF_3) simultaneously. The quality of these fits is satisfactory; *e.g.*, for $\Lambda_{\overline{MS}} = 211$ MeV and $G(x) = A(1-x)^{\prime}$, the PQCD precitions fit the F_2 data well as illustrated in Fig.12. Our F_2 data resolves some of the earlier controversies concerning QCD evolution of F_2 in nuclear targets.[2] The full QCD fit to F_2, with $Q^2 > 5$ GeV^2 cut, is shown in Fig.13 — we observe satisfactory agreement between the data and theory. The values of $\Lambda_{\overline{MS}}$ from F_2 fits are consistent with Eq.9. It must be pointed out that any value of $\Lambda_{\overline{MS}}$ from such a fit is correlated with the x-dependences of the gluon and antiquark distributions. The agreement of the Q^2 evolution of F_2 and xF_3 with PQCD bodes well for a combined analysis, or simultaneous evolution, of the two structure functions leading to a better understanding of the gluon structure function and its evolution.

7: Conclusion

We have presented precision measurements of the nucleon structure functions F_2

Table 4: The Mean-Square Charge Test with $Q^2 > 5$ GeV^2: The average ratio, as in Eq.10, for μ- to the CCFR ν-data is presented. The ratio is evaluated in the Q^2 range overlapping with that of the CCFR data. The Q^2-range spanned by the CCFR data is a superset of all the μ-experiments. The absolute normalization errors of the BCDMS and EMC data are ± 0.03 are ± 0.05 respectively; that of the CCFR data (the denominator) is 2.5%.

Experiment	Ratio	Stat. Error	Syst. Error
BCDMS-C	1.018	±0.002	±0.012
BCDMS-'D'	1.000	±0.002	±0.012
EMC-Fe	0.921	±0.002	±0.023

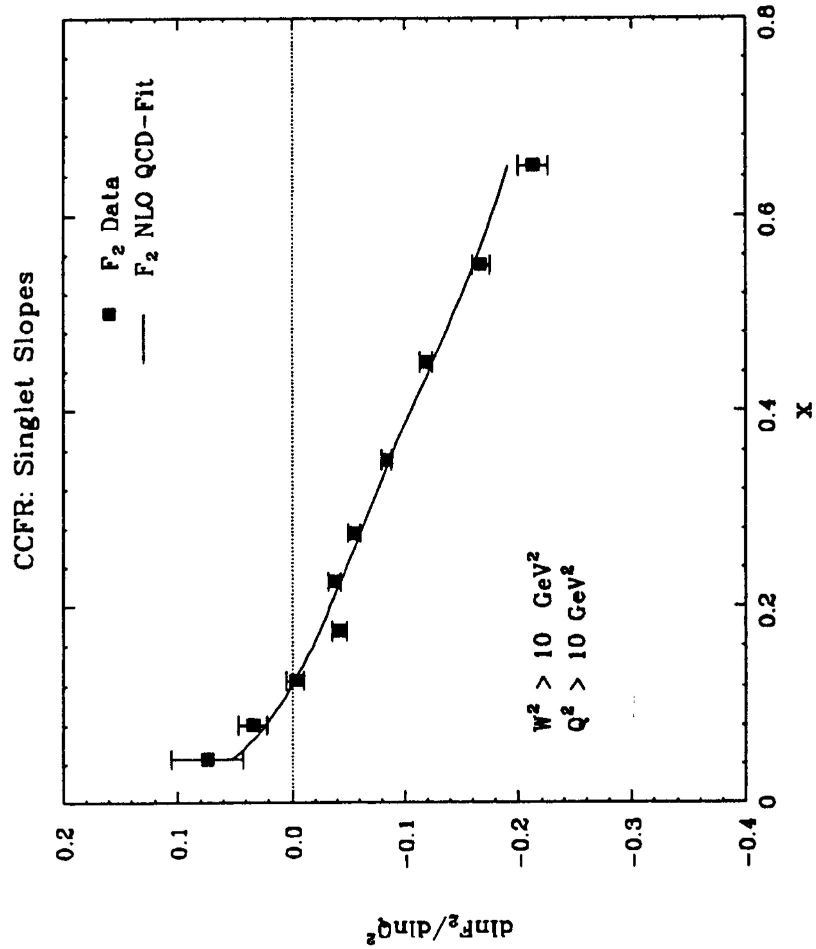

Figure 12: The slopes of F_2 ($= \frac{d\ln F_2}{d\ln Q^2}$) for the CCFR data are shown(squares). The curve is a prediction from perturbative QCD

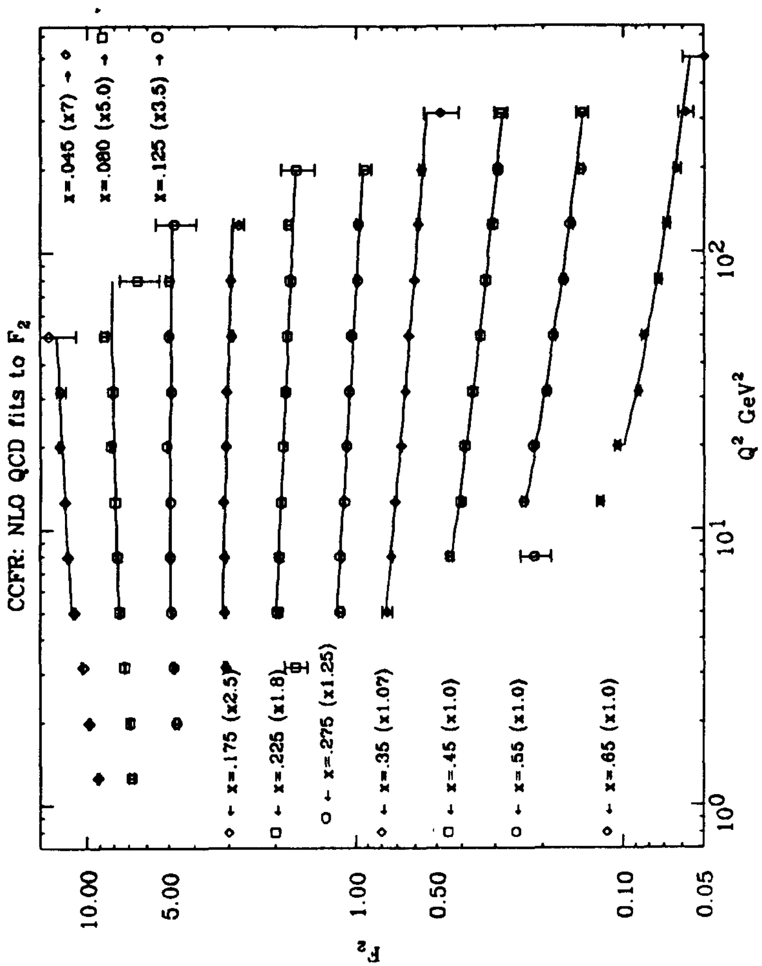

Figure 13: The F_2 data and the best PQCD fit. Cuts of $Q^2 > 5$ GeV^2 and $x < 0.7$ were applied for a next-to-leading order fit including target mass corrections.

and xF_3 spanning a large range of Q^2. The absolute level of the xF_3 data agree with that of CDHSW data; however, the Q^2-dependences disagree. This discrepancy is also seen in F_2. In contrast, the CCFR data show a less steep Q^2 dependence in the range $0.1 \leq x \leq 0.35$, more consistent with that expected from QCD. The CCFR F_2 data are in good agreement with quark charges when compared with the SLAC-'D', the BCDMS-'D' and C data, but show a disagreement of about 7% when compared to the EMC-Fe. The Q^2 evolution of xF_3 agrees well with the PQCD prediction. The evolution of the non-singlet structure function leads to a precise measurement of $\Lambda_{\overline{MS}} = 213 \pm 29(stat.) \pm 41(syst.)$ MeV. The scaling violation of F_2 data also agree well with the PQCD.

We acknowledge the gracious help from the management and staff of Fermilab, as well as many individuals from our home institutions. This research was funded by the National Science Foundation and the Department of Energy.

References

[1] G.Altarelli and G.Parisi, *Nucl. Phys.* **B126**:298, 1977.

[2] S.R.Mishra and F.Sciulli, *Annu. Rev. Nucl. Part. Sci.* **39**, 259(1989).

[3] S.R.Mishra *et al.*, Nevis Preprint # 1459; submitted to *Phys. Rev. Lett.*

[4] W.C.Leung *et al.*, Nevis Preprint # 1460; submitted to *Phys. Rev. Lett.* Also see W.C.Leung, Ph.D. Thesis, Columbia University, 1991.

[5] P.Z.Quintas *et al.*, Nevis Preprint # 1461; submitted to *Phys. Rev. Lett.* Also see P.Z.Quintas, Ph.D. Thesis, Columbia University, 1991.

[6] W.K.Sakumoto *et al.*, *Nucl. Inst. Meth.* **A294**, 179(1990); B.J.King *et al.*, *Nucl. Inst. Meth.* **A302**, 254(1991).

[7] D.B.MacFarlane *et al.*, *Z.Phys.* **C26**, 1(1984); E.Oltman *et al.*, Accepted for publication in *Z.Phys.C.*

[8] CCFR: R.E.Blair *et al.*, *Phys. Rev. Lett.* **51**, 343(1983); CCFR: P.Auchincloss *et al.*, *Z. Phys.* **C48**, 411(1990).

[9] CDHSW: P.Berge *et al.*, *Z. Phys.* **C35**, 443(1987).

[10] P.Auchincloss *et al.*, *Z.Phys.* **C48**, 411(1990); P.Z.Quintas *et al.*, in preparation. Also see, S.R.Mishra,"Probing Nucleon Structure with ν-N Experiment", Nevis Preprint #1426, review talk presented at the "Workshop on Hadron Structure Functions and Parton Distributions", Fermilab, Batavia, April(1990), World Scientific, Ed.D.Geesaman *et al.*

[11] S.Dasu *et al.*, *Phys. Rev. Lett.* **61**, 1061, 1988; L.W.Whitlow *et al.*, *Phys.Lett.* **B250**, 193(1990).

[12] C.Foudas *et al.*, *Phys. Rev. Lett.* **64**:1207, 1990; M.Shaevitz, review talk at Neutrino '90.

[13] H.Georgi and H.D.Politzer, *Phys. Rev.* **D14**, 1829, 1976; R.M.Barnett, *Phys. Rev. Lett.* **36**, 1163, 1976.

[14] A.De Rújula *et al.*, *Nucl. Phys.* **B154**:394, 1979. We have estimated the effect of using the more detailed radiative correction calculation by D.Yu.Bardin *et al.*, *JINR*-E2-86-260 (1986). The difference between the two corrections was generally very small, except at the lowest ($x = 0.015$) and the highest ($x = 0.65$) x-bins. Our structure function results would, thus, change by a few percent if the Bardin's instead of the De Rújula's calculation were used. In a future publication we shall present our results with Bardin's calculation.

[15] CDHSW: P.Berge *et al.*, *Z. Phys.* **C49**, 187(1991).

[16] D.J.Gross and C.H.Llewyllyn Smith, *Nucl. Phys.* **B14**, 337(1969); W.A.Bardeen *et al.*, *Phys. Rev.* **D18**, 3998 (1978).

[17] B.A.Iijima and R.Jaffe, MIT Preprint CTP993, 1983; R.Jaffe private communication.

[18] Small x events have small angles. The muon angle resolution of the CCFR detector is about 1.3mrad at the mean E_μ of 100GeV; for details see W.K.Sakumoto *et al.*, *Nucl. Inst. Meth.* **A294**, 179(1990).

[19] Our present value of S_{GLS} (2.50) is lower than the earlier preliminary presentations (2.66) [see S.R.Mishra, Talk at Lepton-Photon, 1991, Geneva]. Two small changes in the *assumptions* of the analysis lowered S_{GLS}. These changes, we believe, are more accurate than those employed earlier. See Ref.[7].

[20] S.R.Mishra,"Probing Nucleon Structure with ν-N Experiment", Nevis Preprint

#1426, review talk presented at the "Workshop on Hadron Structure Functions and Parton Distributions", Fermilab, Batavia, April(1990), World Scientific, Ed.D.Geesaman *et al.*

[21] Measurements of S_{GLS}: a)CDHS: J.G.H.deGroot *et al.*, *Phys. Lett.* **B82**, 292(1979); b)CHARM: F.Bergsma *et al.*, *Phys. Lett.* **B123**, 269(1983); c)CCFRR: D.B.MacFarlane *et al.*, *Z.Phys.* **C26**, 1(1984); d)WA25: D.Allasia *et al.*, *Phys.Lett.* **B135**, 231(1984), *ibid*, *Z.Phys.* **C28**, 321(1985).

[22] A.Deveto *et al.*, *Phys. Rev.* **D27**:508, 1983.

[23] SLAC: A.Bodek *et al.*, *Phys.Rev.Lett.* **50**, 1431(1983); **51**, 534(1983).

[24] BCDMS: A.C.Benvenuti *et al.*, *Phys.Lett.* **B237**, 592(1990) (D-target); A.C.Benvenuti *et al.*, *Phys.Lett.* **B195**, 91(1987) (C-target).

[25] EMC: J.J.Aubert *et al.*, **Nucl.Phys. B272**, 158(1986) (Fe Target); J.Ashman *et al.*, **Phys.Lett. B202**, 603(1988) (D Target). The additional low-x deuterium data were obtained from S.J.Wimpenny.